https://doi.org/10.5194/egusphere-2025-2266
Preprint. Discussion started: 28 May 2025

Unequal socioeconomic exposure to drought extremes induced by stratospheric aerosol geoengineering

Weijie Fu[1], Xu Yue[1,*], Chenguang Tian[1], Rongbin Xu[2], Yuming Guo[2]

[1] Jiangsu Key Laboratory of Atmospheric Environment Monitoring and Pollution Control, Collaborative Innovation Center of Atmospheric Environment and Equipment Technology, School of Environmental Science and Engineering, Nanjing University of Information Science & Technology (NUIST), Nanjing, 210044, China.

[2] Climate, Air Quality Research Unit, School of Public Health and Preventive Medicine, Monash University, Melbourne, Australia.

[*]Correspondence to: Xu Yue, yuexu@nuist.edu.cn

https://doi.org/10.5194/egusphere-2025-2266
Preprint. Discussion started: 28 May 2025

Abstract

As global temperature rises, the severity and frequency of droughts are projected to increase. Stratospheric aerosol geoengineering (SAG) has been proposed as a potential solution to reduce surface temperatures, but its effectiveness in alleviating drought extremes remains uncertain. Here, we investigate the global impacts of SAG on drought extremes based on experiments from the Geoengineering Model Intercomparison Project (GeoMIP) and the Geoengineering Large Ensemble Project (GLENS). By 2100, the frequency of drought extremes is projected to increase by 7.33% under a high-emission scenario. SAG implementation reduces this increase by 1.99% (1.80% in GLENS), primarily due to its cooling effects. However, SAG-induced rainfall deficits lead to substantial inequity in drought responses. Countries with less development experience smaller reductions, or even increases, in economic and population exposure to extreme drought, compared to more developed nations. These findings highlight the urgent need for improved SAG design to prevent the exacerbation of climate injustice.

https://doi.org/10.5194/egusphere-2025-2266
Preprint. Discussion started: 28 May 2025

1 INTRODUCTION

Global warming is profoundly shaping the Earth with reduced sea ice(Diffenbaugh et al., 2013), raised sea level(Tebaldi et al., 2021), and increased climatic extremes(Song et al.). Persistent warming has expanded the land area with decreased precipitation but increased evaporation, enhancing the frequency and severity of global drought events(Dai, 2011a; Samaniego et al., 2018; Trenberth et al., 2014). As one of the most destructive and persistently widespread natural disasters, drought can have significant impacts on human survival, the economy, and societal structures(Carrão et al., 2016; Dai, 2013; Yue et al., 2021). During 1970-2019, droughts were responsible for 34% of disaster-related fatalities((Wmo), 2021) and annually erode 12 million hectares of arable land(Diallo, 2008), leading to reduced agricultural yields, increased food prices, and escalated economic instability especially for vulnerable populations(Rusca et al., 2023) .

Mitigating global warming requires reducing anthropogenic GHG emissions. However, due to the inertia of climate system, global temperature responses lag behind emission reductions. Geoengineering, particularly Solar Radiation Management (SRM), has been proposed as a potential climate change mitigation approach(Ricke et al., 2012). The SRM aims to reflect incoming solar radiation back into space(Irvine et al., 2012), reducing global surface temperatures(Irvine et al., 2019). As one type of SRM, stratospheric aerosol geoengineering (SAG) has gained significant attentions due to its cost-effectiveness and practicality(Smith, 2020; Smith and Wagner, 2018). This method introduces reflective aerosols into the stratosphere to increase the Earth's albedo(Pope et al., 2012), mimicking the cooling effects observed after volcanic eruptions(Wilson et al., 1993).

Earth System Models (ESMs) are vital for analyzing climatic impacts and the potential side effect of SRM before its implementation(Macmartin and Kravitz, 2019). The Geoengineering Model Intercomparison Project (GeoMIP)(Kravitz et al., 2011) was established to assess climatic responses to geoengineering using multiple ESMs under various forcing scenarios. In contrast, the Geoengineering Large Ensemble (GLENS) project performed multiple experiments with a single ESM, exploring different injection strategies(Tilmes et al., 2018). Ensemble of these simulations indicated that SAG could alter global hydrological cycle, reducing rainfall and shifting the intertropical convergence zone(Krishnamohan and Bala, 2022). Regionally, the

https://doi.org/10.5194/egusphere-2025-2266
Preprint. Discussion started: 28 May 2025

SAG-induced cooling could offset about 90% of extreme drought risks in Cape Town, South Africa(Odoulami et al., 2020). Such benefits were also confirmed by other regional studies(Abiodun et al., 2021). However, the benefits of SAG on reducing drought extremes remain unclear on the global scale.

In this study, we use ensemble simulations from both GeoMIP6 and GLENS to assess 1) whether SRM can reduce the probability of extreme drought events and 2) whether the benefits are socioeconomically equal. We consider two types of SRM, including G6solar by reducing solar constant and G6sulfur by SAG (see Methods). The self-calibrating Palmer Drought Severity Index (scPDSI) is employed to measure drought levels, due to its ability to depict drought state through dynamically calculated climatic thresholds adapted to regional environment(Dai, 2011b; Wells et al., 2004). We quantify changes in the probability of drought extremes with and without SRM interventions under the same warming scenario, which is set to Shared Socioeconomic Pathway 5 (SSP5-8.5) assuming a strong warming future with radiative forcing reaching 8.5 W m^{-2} by the end of this century. We explore the uncertainties associated with different SAG strategies, including the fixed equatorial injection approach adopted by G6sulfur from GeoMIP and the multi-latitude aerosol placement used in GLENS. We pay special attentions to the possible disparity of drought responses to the SAG among countries with different socioeconomic development.

2 METHOD

2.1 Model data

We use outputs from multiple models participating in the G6solar and G6sulfur experiments (Table S1). The G6sulfur experiment involves the linear injection of sulfur dioxide (SO_2) along a latitude band of 10°S-10°N at the height between 18 and 20 km from the year 2020. The SO_2 injection rate is adjusted annually or every decade to lower the global mean surface air temperature from the high forcing scenario (SSP5-8.5) to the medium forcing scenario (SSP2-4.5)(Kravitz et al., 2015). This scheme aims to achieve a more uniform global distribution of sulfate aerosols compared to the single-point injections(English et al., 2012). For some models, prescribed sulfate distribution in stratosphere is applied. As a comparison, G6solar experiment directly reduces the solar constant in an idealized manner to achieve the same reduction in radiative forcing from the high to medium scenario(Kravitz et al., 2015).We use historical simulations

https://doi.org/10.5194/egusphere-2025-2266
Preprint. Discussion started: 28 May 2025

and future projections under the SSP5-8.5 scenario to assess the mitigating effects of different SRMs. Some models provide multiple realizations for both historical and SSP5-8.5 experiments. We analyze data only from ensemble members that have the same realizations in both the G6sulfur and G6solar experiments. As a result, we select five available climate models participating in the GeoMIP6 experiment (Table S1) with qualified outputs to calculate changes in drought state from the present day to the end of the 21st century. All model data with varied spatial resolutions are interpolated to the same grid of 1°×1° to facilitate the calculation of multi-model ensemble mean. Inter-model consistency was evaluated based on the number of models that aligned with the direction of the multi-model ensemble change. Changes in the multi-model ensemble were deemed robust if more than four models exhibited changes with the same sign; otherwise, these changes were considered uncertain.

To evaluate the robustness of our findings, we conducted a comparative analysis with the Geoengineering Large Ensemble Project (GLENS)(Tilmes et al., 2018). Unlike the idealized equatorial injection strategy employed in G6sulfur, GLENS implements a feedback-control algorithm designed to maintain global mean surface temperature, interhemispheric temperature gradients, and equator-to-pole temperature gradients at 2020 levels under a high-emission RCP8.5 scenario(Kravitz et al., 2017). This approach dynamically adjusts sulfate aerosol injection rates in different locations based on predefined temperature targets(Macmartin et al., 2017). The GLENS dataset consists of a 20-member ensemble generated by the NCAR Community Earth System Model (CESM1), which incorporates the Whole Atmosphere Community Climate Model (WACCM) as its atmospheric component (Table S2). Our analysis exclusively considered ensemble members with continuous simulations spanning the entire 21st century across both feedback and control experiments (001, 002, and 003). This comparative framework allows us to assess the sensitivity of drought extremes and socioeconomic exposure to different SAG deployment strategies.

2.2 Socioeconomic data and exposure

We use Gross Domestic Product (GDP) data(Geiger, 2018) with a spatial resolution of 0.25° from 2000 to 2020, along with GDP projections for 2025-2100 under the SSP5-8.5 scenario(Dellink et al., 2017) . The GDP values are standardized to the 2005 purchasing power parity (PPP) international dollar for comparability(Wang and Sun,

https://doi.org/10.5194/egusphere-2025-2266
Preprint. Discussion started: 28 May 2025

2022; Geiger, 2018). Population data at 1-km resolution, including urban, rural, and total populations, are sourced from the Socioeconomic Data and Applications Center (SEDAC) for five-year intervals from 2000 to 2020(Jones and O'neill, 2020) . For future projections, we use population data at ten-year intervals and one-eighth degree resolution in space under the SSP5-8.5 scenario for 2020-2100(Jones and O'neill, 2016, 2020). The GDP (or population) exposure is calculated as the frequency of extreme drought multiplied by the GDP (or population) values in each grid cell(Sun et al., 2022).

The Human Development Index (HDI) from the Human Development Report is used to differentiate the economic development of various countries and regions(Undp, 2024). In total, 158 countries with land area larger than 10000 km^2 (the size of at least one 1°×1° grid) are selected and separated into four HDI groups including low (HDI<0.55), medium (0.55<HDI<0.699), high (0.7<HDI<0.799), and very high (HDI >0.8) levels following the suggested criteria(Undp, 2024). The gridded GDP or population exposure is summed up for each country, and then aggregated into four HDI groups accordingly.

2.3 Drought indices

We use scPDSI as the primary metric to quantify the spatiotemporal variations of drought events. The scPDSI is calculated separately for each model with the corresponding meteorological variables. At each grid, monthly precipitation and potential evapotranspiration (PET, mm/day) are used to assess drought severity based on dynamically computed thresholds from historical reference period climates(Wells et al., 2004). There are two common methods for calculating PET: the Penman-Monteith and Thornthwaite parameterization schemes(Thornthwaite, 1948; Penman and Keen, 1948; Monteith, 1965). In this study, we use the Penman-Monteith equation, which calculates PET base on surface air temperature (*T*, °C), net surface radiation (*Rn*, MJ day^{-1} m^{-2}), surface specific humidity (*q*, kg/kg), two-meter wind speed (*U*, m/s), and surface air pressure (*p*, kPa):

$$PET_{pm} = \frac{\Delta \cdot Rn + 6.43\gamma(1 + 0,.536U)(e_s - e_a)}{(\Delta + \gamma)\lambda} \qquad (Equation\ 1)$$

where Δ is the slope of the saturation vapor pressure curve, γ is psychrometric coefficient, λ is latent heat of vaporization, $(e_s - e_a)$ is the saturation vapor pressure

https://doi.org/10.5194/egusphere-2025-2266
Preprint. Discussion started: 28 May 2025

deficit, which can be calculated by air temperature, specific humidity, and air pressure at the surface:

$$e_s - e_a = 0.6112e^{\left(17.62T/(243.12+T)\right)} - \frac{p \cdot q}{q + 0.622(1-q)} \qquad (Equation\ 2)$$

Since CMIP6 provides wind speeds at 10 meters above the surface, we convert them to wind speed at 2 meters(Allan et al., 1998):

$$U_2 = \frac{4.87}{\ln\,(67.8 * z - 5.42)} U_{10} \qquad (Equation\ 3)$$

Here z = 10 meters. The original drought index, PDSI, is calculated using fixed climatic thresholds that are not comparable across different climatic regions. To address such limitation, the scPDSI employs dynamic thresholds based on the regional environment, offering the advantage of both spatial and temporal comparability(Wells et al., 2004; Dai, 2011b; Van Der Schrier et al., 2013).

The standard scPDSI values range from -4 to 4, representing conditions from extremely dry to extremely wet. In this study, an extreme drought month is defined if scPDSI value is lower than -4. The frequency of drought extremes for a given scenario is calculated as the fraction of extreme drought months out of a 240-month period. Additionally, we compute other drought indices for comparisons, including the PDSI, Palmer Modified Drought Index (PMDI), Palmer Hydrological Drought Index (PHDI), and Palmer Z Index (Z-index).

2.4 Mitigation Potential (MP)

We define the MP value to quantify the extent to which SRM could mitigate the increased drought risks induced by climate warming:

$$MP = \frac{P_{SRM} - P_{SSP585}}{P_{SSP585} - P_{hist}} \qquad (Equation\ 4)$$

Here, P_{hist} represents the exposure (either GDP or population) to drought extremes (scPDSI < -4) at present day averaged for the period of 1995-2014. P_{SSP585} and P_{SRM} represent the mean drought exposure at 2081-2100 under the SSP5-8.5 and SRM (G6solar or G6sulfur) scenarios, respectively. We calculate the MP values for four different HDI groups of countries by summing the GDP or population exposure within each HDI group. For individual countries, we calculate the MP values based on the GDP or population exposure for that specific country. Our analyses showed that the denominator of Equation (4) is positive for all four HDI groups and for 96% of the 158

https://doi.org/10.5194/egusphere-2025-2266
Preprint. Discussion started: 28 May 2025

countries, indicating that drought exposure is projected to increases in the future under the SSP5-8.5 scenario. A negative MP value indicates that SRM helps mitigate the warming-induced increase of drought exposure, and vice versa. The units of the MP value can be expressed as a percentage (when MP<1) or as a ratio (when MP>1).

2.5 Drought Exposure Disparity (DED)

The DED values are defined to assess the disparity of drought exposure among countries with different HDI:

$$DED = \frac{P_{low\ HDI}}{P_{very\ high\ HDI} + P_{high\ HDI}} \qquad (Equation\ 5)$$

Here, $P_{low\ HDI}$ represents the sum of the exposure (GDP or population) to drought extremes (scPDSI < -4) for all low HDI countries. $P_{very\ high\ HDI}$ and $P_{high\ HDI}$ are exposures in very high HDI countries and high HDI countries, respectively. An increase of DED indicates an enhanced inequality for the socioeconomic exposure to drought extremes.

2.6 Numerical experiments

For each climate model, we collect monthly temperature, precipitation, and radiation to calculate historical scPDSI using present-day climatic variables and future scPDSI using meteorology from the SSP5-8.5, G6sulfur, or G6solar scenarios (Table S3). To identify the main drivers of scPDSI changes, we perform 6 additional sensitivity experiments by combining historical meteorological forcings with future projections under the SSP5-8.5, G6sulfur, or G6solar scenarios (Table S3). In these experiments, we replace one variable at a time from the SSP5-8.5 scenario with the corresponding future projections from GeoMIP6 scenarios. The differences in scPDSI between sensitivity experiments and the full sets of future projections (SSP5-8.5 or GeoMIP) indicate the contributions of individual climatic forcing to the changes of scPDSI. We select 1995-2014 as the historical reference period and 2081-2100 as the future projection period for analyses.

2.7 Model evaluations

Monthly precipitation and temperature from the CRU TS (Climate Research Unit Gridded Time Series) dataset version 4.07 are used to evaluate the model's performance

https://doi.org/10.5194/egusphere-2025-2266
Preprint. Discussion started: 28 May 2025

in reproducing present-day climate(Harris et al., 2020). Both the CRU data and model output are interpolated to 1°×1°. We calculate the correlation coefficient (R, 1 is best), standard deviation ratio (SDEV, 1 is best), and centered root-mean-square error (CRMSE, 0 is best) between the CRU data and model simulations(Taylor, 2001). For temperature, all models reproduce the observed spatial pattern with R>0.98 and SDEV ranging from 0.95 to 1.08 (Fig S1a). The CRMSE for most modes is less than 2, except for IPSL-CM6A-LR (2.24). For precipitation, R ranges from 0.74 to 0.85, SDEV ranges from 0.82 to 1, and CRMSE ranges from 0.99 to 1.55 (Fig S1b). Although the R for simulated precipitation is lower than that for temperature, the CRMSE is generally lower. Overall, the selected models reasonably reproduce the observed meteorology with low biases. While all models accurately capture the changing characteristics of temperature and precipitation, differences in parameterization schemes for radiation, cloud-aerosol interactions, aerosol microphysics, and other factors result in variations in the simulated patterns of meteorological factors(Mauritsen et al., 2019; Visioni et al., 2021). Therefore, we use the multi-model ensemble to minimize biases caused by inter-model variations.

3 RESULTS

3.1 Responses of temperature and precipitation to SRM

By the end of 21st century, global surface air temperature is projected to increase by 4.26°C under the SSP5-8.5 scenario relative to 1995–2014 (Fig 1a). Such warming is more significant at the mid-to-high latitudes in Northern Hemisphere (NH). The pronounced temperature rise intensifies hydrological cycle, evidenced by enhanced water vapor content in lower troposphere(Held and Soden, 2006), resulting in an increased global average precipitation of 0.19 mm/day (Fig 1d). However, a discernible reduction of rainfall is noted in regions including northern South America, southern Africa, Australia, southern North America, and western Europe.

Reduction of the solar constant in G6solar causes a uniformly distributed cooling worldwide (Fig 1b), counteracting 46.5% of the warming in SSP5-8.5. For G6sulfur, the injection of sulfur aerosols (or SO_2) contributes to a reduction in global average surface temperature of about -1.84°C (Fig 1c), slightly weaker than that of G6solar. Although both SRMs mitigate less than half of the temperature rise, they offset most of the increase in precipitation attributable to global warming (Fig 1e and 1f)(Niemeier et

https://doi.org/10.5194/egusphere-2025-2266
Preprint. Discussion started: 28 May 2025

al., 2013; Ricke et al., 2023). Such responses of precipitation are markedly uneven in space, as reflected by significant heterogeneity in precipitation distribution patterns(Zhang et al., 2024; Simpson et al., 2019). The SRM-induced tropospheric cooling weakens tropical circulation, inhibiting convection and subsequently reducing precipitation(Ferraro et al., 2014). Notably, the G6sulfur shows most prominent rainfall deficit in central Africa and Indonesia due to the weakening of the monsoon circulation and shifting of the monsoon precipitation distribution(Bonou et al., 2023). This reduction in precipitation is more pronounced in the GLENS simulations (Fig S2d), driven by the stronger cooling (Fig S2b) from the larger sulfur injection(Krishnamohan and Bala, 2022).

3.2 Responses of drought extremes to SRM

Following the intense warming, frequency of extreme drought events increases by 7.33% globally under the SSP5-8.5 scenario (Fig 2a). Such an enhancement is more pronounced at the mid-to-high latitudes, especially in the southern hemisphere (e.g., Australia and southern Africa) where precipitation is projected to decrease (Fig 1d). In contrast, the wet tendencies in some tropical areas (e.g., India and central Africa) and boreal regions outweigh the local warming, resulting in alleviated drought stresses at the low or high latitudes of both hemispheres.

The SRM shows good potentials to decrease extreme drought occurrences. With the implementation of G6solar, frequency of extreme drought events is reduced by 2.12% globally (Fig 2d), mitigating 28.9% of the increased drought stress under the SSP5-8.5 scenario (Fig 2a). Regionally, drought extremes are projected to decline uniformly at most latitudes, with stronger amelioration over Europe, Australia, and southern Africa where precipitation increases by G6solar (Fig 1e). With G6sulfur, a similar reduction of -1.99% is predicted for global drought extremes but with large spatial heterogeneity (Fig 2g). Most of such reductions are located in the Southern Hemisphere, especially over Australia and southern Africa. In contrast, the frequency of drought extremes enhances significantly in central Africa, following the G6sulfur-induced precipitation deficit (Fig 1f). This region has been enduring prolonged droughts since the 1990s, demonstrating high vulnerability to climate change impacts(Palmer et al., 2023; Kendon et al., 2019; Zhou et al., 2014). The SAG in GLENS exhibited mitigation efficacy comparable to that of G6sulfur in reducing the frequency of extreme droughts,

https://doi.org/10.5194/egusphere-2025-2266
Preprint. Discussion started: 28 May 2025

but it also led to increased drought probability in central Africa, India, and northern Asia (Fig S3).

3.3 Attribution of extreme drought response to SRM

We performed sensitivity experiments to elucidate the causes of extreme drought variations. Under the SSP5-8.5 scenario, changes in temperature and radiation lead to an increased frequency of extreme drought events compared to the historical period (Fig 2b). Significant warming (Fig 1a) enhances the frequency of extreme droughts globally by 5.43%, with the most pronounced increases in the mid- and high-latitudes of the Northern Hemisphere (NH, Fig S4a). By the end of the century, radiation increases by 0.25 W m^{-2} due to the reduction of anthropogenic aerosols(Hodnebrog et al., 2024), intensifying potential evapotranspiration (PET) and worsening drought conditions (Fig S4g). In contrast, the increase in global precipitation (Fig 1d) under the SSP5-8.5 scenario reduces the frequency of drought extremes by 2.12% globally and across most regions, except for southern Africa, Australia, and western Europe (Fig S4d). On the global scale, warming is the dominant factor driving changes in drought extremes over 50.17% of land area (excluding ice and desert), surpassing the 47.97% influenced by precipitation (Fig 2c).

Relative to SSP5-8.5, SRM-induced cooling reduces extreme drought frequency by 3.44% in G6solar (Fig 2e) and 3.42% in G6sulfur (Fig 2h). This mitigation shows a very similar spatial pattern between the two SRMs, with a more pronounced effect at mid-high latitudes in the NH (Fig S4b and S4c). Additionally, the reduction of solar radiation due to dimming effects further alleviates global drought extremes by 0.85% for G6solar (Fig 2e) and 1.42% for G6sulfur (Fig 2H). However, SRM-induced rainfall deficits (Figs 1e and 1f) increase the frequency of extreme drought by 1.61% for G6solar and 2.12% for G6surfur relative to SSP5-8.5 scenario, with the most significant impacts occurring in central Africa where the reduction in precipitation is at its maximum (Fig S4e and S4f). These changes partly offset the cooling-induced mitigation, resulting in patchy responses of drought extremes in the NH (Fig 2d and 2g). Compared to G6solar, the rainfall deficit is larger in G6sulfur, leading to an enhanced frequency of drought extremes in central Africa, the eastern U.S., and eastern Europe. Consequently, changes in precipitation act as the dominant driver of drought over more land areas in G6sulfur (Fig 2i) than that in G6solar (Fig 2f). Exceptions are

https://doi.org/10.5194/egusphere-2025-2266
Preprint. Discussion started: 28 May 2025

found in southern Africa and Australia, where lower temperatures and higher precipitation collectively reduce extreme drought events.

3.4 Global socioeconomic disparity in exposure to drought extremes

To assess the impacts of future warming and the implementation of SRM on human societal development, we analyzed variations of global GDP and population exposure to drought extremes across different scenarios. Compared to present day, there are significant increases of $72.1 trillion in GDP and 460 million in population exposed to extreme drought every year by the end of century under the SSP5-8.5 scenario (Fig 3a and 3d). High exposure areas are located in eastern North America, western Europe, and eastern China. As an effective mitigation, G6solar can reduce annual GDP exposure by $18.6 trillion and population exposure by 142 million people to extreme drought (Fig 3b and 3e), resulting in the mitigation potential (MP, see Methods) of -25.8% for GDP and -30.9% for population (Fig 3b and 3e). As a comparison, the MP of G6sulfur is lower at -17.9% for GDP and -22.5% for population (Fig 3c and 3f). The SAG in GLENS achieves a similar global MP of -19.6% in GDP to that in G6sulfur (Fig S5b). However, it results in a 15.9% increase in global population exposure to extreme drought relative to SSP5-8.5, mainly because of the substantial enhancement of drought risks in India, central Africa, and eastern China (Fig S5d).

The spatial heterogeneity of these mitigations result in pronounced disparities among countries with different Human Development Indices (HDI). G6solar reduces GDP exposure to drought extremes by 35.1% in very high HDI countries and by 19.9% in high HDI countries, but only 11.2% in countries with low HDI (Fig 4a). This disparity becomes even more pronounced under the G6sulfur scenario, in which the frequency of GDP exposure to drought extremes instead increases by 12.6% relative to SSP5-8.5 for low HDI countries, with the highest risks in South Sudan, Rwanda, and Burundi (Fig 4e). Both SRMs result in relatively weaker MP for population exposure compared to GDP in low and medium HDI countries, with G6sulfur even increasing population exposure by up to 42.9% in low HDI countries. Similar to GDP, the top 5 countries suffering the largest increases in population exposure are located in central Africa (Fig 4f). As a comparison, the SAG in GLENS shows pronounced risk amplification, with notably elevated risks of drought exposure for medium- and low-HDI countries compared to the SRM approaches in GeoMIP (Fig 4a-b). We use the

https://doi.org/10.5194/egusphere-2025-2266
Preprint. Discussion started: 28 May 2025

index of drought exposure disparity (DED, see Methods) to indicate the inequity of drought exposure between high- and low-HDI countries. Compared to SSP5-8.5, G6solar increases the DED of GDP by 12.72% and that of population by 30.58%. Under G6sulfur, this disparity is even more pronounced, with DED values increasing by 22.74% for GDP and 36.34% for population, with GLENS experiment increasing 244.37% for GDP and 251.18% for population.

4 DISCUSSION

Global warming is projected to enhance future drought risks(Dai, 2013). SRM is hypothesized to partially offset warming, but its regional climatic and societal impacts remain uncertain(Irvine et al., 2019). Our analyses show asymmetric responses in temperature and precipitation to SRM, resulting in limited effectiveness of SRM in alleviating global drought extremes under a high emission scenario. While the SRM in GeoMIP mitigates less than half of the warming, it offsets more than 70% of the rainfall enrichment under the SSP5-8.5 scenario (Fig 1). This is because SRM-induced surface cooling increases atmospheric stability, weakens global hydrological cycle, and reduces land precipitation especially over monsoon regions(Krishnamohan and Bala, 2022; Tilmes et al., 2013), such as India and China (Fig 1e). Relative to G6solar, precipitation is even more inhibited in G6sulfur especially over central Africa (Fig 1f), because the absorbing sulfate aerosols induces an anomalous stratospheric heating that further enhances air stability(Simpson et al., 2019; Tilmes et al., 2022). In addition, SAG overcompensates for the greenhouse gas-forced expansion of the Hadley Circulation(Cheng et al., 2022) and offsets the poleward shift of storm tracks in the mid-latitude of NH(Karami et al., 2020). These changes, along with a more positive phase of the North Atlantic Oscillation induced by SAG(Jones et al., 2022), resulting in increased exposures to drought in Europe and the northeastern U.S. (Fig 3c and 3f).

Previous studies have revealed the negative impacts of SAG on hydrological cycles, but they mainly highlighted the benefits of SAG in mitigating temperature and precipitation extremes induced by climate warming(Irvine et al., 2019; Jones et al., 2017). However, variations of drought involve complex relationships between temperature and precipitation, leading to nonlinear responses of drought to the perturbations in these climatic variables. For instance, the sum of the contributions of individual climatic factors is not equal to the total changes in drought extremes under

https://doi.org/10.5194/egusphere-2025-2266
Preprint. Discussion started: 28 May 2025

the SSP5-8.5 and two SRM scenarios (Fig 2 and S4). Few studies have explored the SAG impacts on global drought using specific drought indices(Liu et al., 2024; Abiodun et al., 2021), but they tend to focus on the mean state of drought events rather than drought extremes. Our additional analyses showed very limited changes in the mean scPDSI values for both G6solar and G6sulfur relative to the SSP5-8.5 scenario on the global scale (Fig S6a-S6c). The regional reduction (indicating a drier state) of scPDSI by G6sulfur is also smaller in magnitude than the increase (indicating a wetter state) under SSP5-8.5 over central Africa, masking the unbalanced responses as shown for the drought extremes (Fig 2).

The climatic effects of SAG vary depending on the intensity and deployment strategies. Under the same high-emission scenario, the GeoMIP SAG (G6sulfur) experiment aims to limit global warming to a moderate level, whereas GLENS implements SAG intensively to offset all the warming(Tilmes et al., 2018; Tilmes et al., 2015). Furthermore, these two experiments employ distinct injection methodologies, with the multi-latitude aerosol deployment in GLENS but fixed equatorial injection in GeoMIP. Despite these differences, both GLENS and GeoMIP exhibit similar spatial patterns in their impacts on extreme drought (Fig 2g and S3b). This similarity suggests that the choice of injection strategy does not substantially alter the major conclusions, which highlight the increased spatial heterogeneity in drought responses under the SAG implementation. However, regional differences, particularly in India and northern China, lead to different levels of extreme drought risk for the global economy and population.

Our findings are subject to some limitations and uncertainties. First, differences in model configurations may affect the predicted impacts of SRM. For instance, the IPSL-CM6A-LR and UKESM1-0-LL models simulate changes in stratospheric chemistry by using actual injected SO_2, whereas CNRM-ESM2-1 and MPI-ESM1.2 employ prescribed distributions of stratospheric aerosol(Niemeier et al., 2020; Tilmes et al., 2015; Visioni et al., 2021). Although each model predicts comparable cooling effects, variations in the SAG implementation may lead to discrepancies in precipitation perturbations that are vital for predicting drought responses. Here, we employed a multi-model ensemble to derive climatic changes that are consistent among the majority of models. Second, the application of a single drought index may influence the projection results. For this study, we used scPDSI due to its clear physical meaning,

https://doi.org/10.5194/egusphere-2025-2266
Preprint. Discussion started: 28 May 2025

adaptive climatic responses, and specific criteria for drought extremes(Wells et al., 2004). As a comparison, we checked other drought indices such as PDSI, Palmer Modified Drought Index (PMDI), Palmer Hydrological Drought Index (PHDI), and Palmer Z Index (Z-index). Projections using these indices showed similar patterns to scPDSI though with spatially varied magnitude (Fig S6), suggesting that our main conclusions are not affected by the selection of the drought index. Third, uncertainties in future projections of GDP and population may affect exposure to drought extremes. In this study, we applied the future estimates of GDP and population density from the SSP5-8.5 scenario by the end of the 21st century. As a check, we used present-day economic and population data to predict future changes in drought exposure. Although the specific numbers changed, we found similar spatial variations in drought exposure using either present-day (Fig S7) or future (Fig 3) GDP and population data. The main conclusion remains that low HDI countries bear the largest exacerbation in both economic and population exposures to drought extremes due to SAG (Fig S8).

Despite these limitations, our multi-model ensemble projection presents a strong impact of SAG on global drought extremes and the consequent exposures for economy and population. As an effective intervention for global warming, SAG exhibits certain potentials in mitigating drought risks but with large spatial heterogeneity. Particularly, this study emphasizes the heightened vulnerability of low HDI countries to exacerbated drought exposures due to SAG. Future projections indicate that these regions, already at a socio-economic disadvantage, will face the most severe impacts on both economic development and public health. This spatial disparity underscores the importance of considering equity and regional specificities in SAG policies. As we navigate the complexities of geoengineering, it is imperative to weigh the global benefits against the localized risks, ensuring that strategies do not disproportionately burden the most vulnerable regions.

Financial support

This study was jointly funded by the National Key Research and Development Program of China (2023YFF0805402) and Natural Science Foundation of Jiangsu Province (BK20220031).

Competing interests

The authors declare no conflicts of interest relevant to this study.

https://doi.org/10.5194/egusphere-2025-2266
Preprint. Discussion started: 28 May 2025

Data and code availability

The datasets are downloaded from the Coupled Model Intercomparison Project phase six (CMIP6, https://esgf-node.llnl.gov/search/cmip6/) and Geoengineering Large Ensemble Project (GLENS, https://www.cesm.ucar.edu/community-projects/glens) for simulated meteorology, and Climate Research Unit Gridded Time Series version4.07 (CRU TS4.07, https://crudata.uea.ac.uk/cru/data/hrg/) for observed meteorology. Population data are collected from Socioeconomic Data and Applications Center (SEDAC, https://sedac.ciesin.columbia.edu/). HDI data are from United Nations Development Programme (UNDP, https://hdr.undp.org/). Code for calculating scPDSI can be found at https://climate-indices.readthedocs.io/en/latest/.

ACKNOWLEDGMENTS

The authors thank the CMIP6 for providing the GeoMIP6 datasets and the NCAR for the GLENS datasets. This study was jointly funded by the National Key Research and Development Program of China (2023YFF0805402) and Natural Science Foundation of Jiangsu Province (BK20220031).

https://doi.org/10.5194/egusphere-2025-2266
Preprint. Discussion started: 28 May 2025

REFERENCES

(WMO), W. M. O.: Atlas of mortality and economic losses from weather, climate and water extremes (1970–2019), WMO, Geneva :, 90 p. pp.2021.

Abiodun, B. J., Odoulami, R. C., Sawadogo, W., Oloniyo, O. A., Abatan, A. A., New, M., Lennard, C., Izidine, P., Egbebiyi, T. S., and MacMartin, D. G.: Potential impacts of stratospheric aerosol injection on drought risk managements over major river basins in Africa, Climatic Change, 169, 31, https://doi.org/10.1007/s10584-021-03268-w, 2021.

Allan, R., Pereira, L., and Smith, M.: Crop evapotranspiration-Guidelines for computing crop water requirements-FAO Irrigation and drainage paper 56, 1998.

Bonou, F., Da-Allada, C. Y., Baloitcha, E., Alamou, E., Biao, E. I., Zandagba, J., Obada, E., Pomalegni, Y., Irvine, P. J., and Tilmes, S.: Stratospheric Sulfate Aerosols Impacts on West African Monsoon Precipitation Using GeoMIP Models, Earth's Future, 11, e2023EF003779, https://doi.org/10.1029/2023EF003779, 2023.

Carrão, H., Naumann, G., and Barbosa, P.: Mapping global patterns of drought risk: An empirical framework based on sub-national estimates of hazard, exposure and vulnerability, Global Environmental Change, 39, 108-124, https://doi.org/10.1016/j.gloenvcha.2016.04.012, 2016.

Cheng, W., MacMartin, D. G., Kravitz, B., Visioni, D., Bednarz, E. M., Xu, Y., Luo, Y., Huang, L., Hu, Y., Staten, P. W., Hitchcock, P., Moore, J. C., Guo, A., and Deng, X.: Changes in Hadley circulation and intertropical convergence zone under strategic stratospheric aerosol geoengineering, npj Climate and Atmospheric Science, 5, 32, 10.1038/s41612-022-00254-6, 2022.

Dai, A.: Drought under global warming: a review, WIREs Climate Change, 2, 45-65, https://doi.org/10.1002/wcc.81, 2011a.

Dai, A.: Characteristics and trends in various forms of the Palmer Drought Severity Index during 1900–2008, Journal of Geophysical Research, 116, https://doi.org/10.1029/2010JD015541, 2011b.

Dai, A.: Increasing drought under global warming in observations and models, Nature Climate Change, 3, 52-58, https://doi.org/10.1038/nclimate1633, 2013.

Dellink, R., Chateau, J., Lanzi, E., and Magné, B.: Long-term economic growth projections in the Shared Socioeconomic Pathways, Global Environmental Change, 42, 200-214, https://doi.org/10.1016/j.gloenvcha.2015.06.004, 2017.

Diallo, H. A.: United Nations convention to Combat desertification (UNCCD), The Future of Drylands: International Scientific Conference on Desertification and Drylands Research Tunis, Tunisia, 19-21 June 2006, 13-16,

Diffenbaugh, N. S., Scherer, M., and Ashfaq, M.: Response of snow-dependent hydrologic extremes to continued global warming, Nature Climate Change, 3, 379-384, 10.1038/nclimate1732, 2013.

English, J. M., Toon, O. B., and Mills, M. J.: Microphysical simulations of sulfur burdens from stratospheric sulfur geoengineering, Atmospheric Chemistry and Physics., 12, 4775-4793, 10.5194/acp-12-4775-2012, 2012.

Ferraro, A. J., Highwood, E. J., and Charlton-Perez, A. J.: Weakened tropical circulation and reduced precipitation in response to geoengineering, Environmental Research Letters, 9, 014001, 10.1088/1748-9326/9/1/014001, 2014.

Geiger, T.: Continuous national gross domestic product (GDP) time series for 195 countries: past observations (1850–2005) harmonized with future projections according

https://doi.org/10.5194/egusphere-2025-2266
Preprint. Discussion started: 28 May 2025

to the Shared Socio-economic Pathways (2006–2100), Earth System. Science. Data, 10, 847-856, 10.5194/essd-10-847-2018, 2018.

Harris, I., Osborn, T. J., Jones, P., and Lister, D.: Version 4 of the CRU TS monthly high-resolution gridded multivariate climate dataset, Scientific Data, 7, 109, 10.1038/s41597-020-0453-3, 2020.

Held, I. M. and Soden, B. J.: Robust Responses of the Hydrological Cycle to Global Warming, Journal of Climate, 19, 5686-5699, https://doi.org/10.1175/JCLI3990.1, 2006.

Hodnebrog, Ø., Myhre, G., Jouan, C., Andrews, T., Forster, P. M., Jia, H., Loeb, N. G., Olivié, D. J. L., Paynter, D., Quaas, J., Raghuraman, S. P., and Schulz, M.: Recent reductions in aerosol emissions have increased Earth's energy imbalance, Communications Earth & Environment, 5, 166, 10.1038/s43247-024-01324-8, 2024.

Irvine, P., Emanuel, K., He, J., Horowitz, L. W., Vecchi, G., and Keith, D.: Halving warming with idealized solar geoengineering moderates key climate hazards, Nature Climate Change, 9, 295-299, 10.1038/s41558-019-0398-8, 2019.

Irvine, P. J., Sriver, R. L., and Keller, K.: Tension between reducing sea-level rise and global warming through solar-radiation management, Nature Climate Change, 2, 97-100, 10.1038/nclimate1351, 2012.

Jones, A., Haywood, J. M., Scaife, A. A., Boucher, O., Henry, M., Kravitz, B., Lurton, T., Nabat, P., Niemeier, U., Séférian, R., Tilmes, S., and Visioni, D.: The impact of stratospheric aerosol intervention on the North Atlantic and Quasi-Biennial Oscillations in the Geoengineering Model Intercomparison Project (GeoMIP) G6sulfur experiment, Atmospheric Chemistry and Physics, 22, 2999-3016, 10.5194/acp-22-2999-2022, 2022.

Jones, A. C., Haywood, J. M., Dunstone, N., Emanuel, K., Hawcroft, M. K., Hodges, K. I., and Jones, A.: Impacts of hemispheric solar geoengineering on tropical cyclone frequency, Nature Communications, 8, 1382, 10.1038/s41467-017-01606-0, 2017.

Jones, B. and O'Neill, B. C.: Spatially Explicit Global Population Scenarios Consistent with the Shared Socioeconomic Pathways, Environmental Research Letters, 2016.

Jones, B. and O'Neill, B. C.: Global One-Eighth Degree Population Base Year and Projection Grids Based on the Shared Socioeconomic Pathways, Revision 01, NASA Socioeconomic Data and Applications Center (SEDAC) [dataset], 2020.

Karami, K., Tilmes, S., Muri, H., and Mousavi, S. V.: Storm Track Changes in the Middle East and North Africa Under Stratospheric Aerosol Geoengineering, Geophysical Research Letters, 47, e2020GL086954, https://doi.org/10.1029/2020GL086954, 2020.

Kendon, E. J., Stratton, R. A., Tucker, S., Marsham, J. H., Berthou, S., Rowell, D. P., and Senior, C. A.: Enhanced future changes in wet and dry extremes over Africa at convection-permitting scale, Nature Communications, 10, 1794, 10.1038/s41467-019-09776-9, 2019.

Kravitz, B., Robock, A., Boucher, O., Schmidt, H., Taylor, K. E., Stenchikov, G., and Schulz, M.: The Geoengineering Model Intercomparison Project (GeoMIP), Atmospheric Science Letters, 12, 162-167, https://doi.org/10.1002/asl.316, 2011.

Kravitz, B., MacMartin, D. G., Mills, M. J., Richter, J. H., Tilmes, S., Lamarque, J.-F., Tribbia, J. J., and Vitt, F.: First Simulations of Designing Stratospheric Sulfate Aerosol Geoengineering to Meet Multiple Simultaneous Climate Objectives, Journal of Geophysical Research: Atmospheres, 122, 12,616-612,634, https://doi.org/10.1002/2017JD026874, 2017.

Kravitz, B., Robock, A., Tilmes, S., Boucher, O., English, J. M., Irvine, P. J., Jones, A., Lawrence, M. G., MacCracken, M., Muri, H., Moore, J. C., Niemeier, U., Phipps, S. J., Sillmann, J.,

https://doi.org/10.5194/egusphere-2025-2266
Preprint. Discussion started: 28 May 2025

Storelvmo, T., Wang, H., and Watanabe, S.: The Geoengineering Model Intercomparison Project Phase 6 (GeoMIP6): simulation design and preliminary results, Geosci. Model Dev., 8, 3379-3392, 10.5194/gmd-8-3379-2015, 2015.

Krishnamohan, K. S. and Bala, G.: Sensitivity of tropical monsoon precipitation to the latitude of stratospheric aerosol injections, Climate Dynamics, 59, 151-168, 10.1007/s00382-021-06121-z, 2022.

Liu, Z., Lang, X., and Jiang, D.: Stratospheric Aerosol Injection Geoengineering Would Mitigate Greenhouse Gas-Induced Drying and Affect Global Drought Patterns, Journal of Geophysical Research: Atmospheres, 129, e2023JD039988, https://doi.org/10.1029/2023JD039988, 2024.

MacMartin, D. G. and Kravitz, B.: Mission-driven research for stratospheric aerosol geoengineering, Proceedings of the National Academy of Sciences, 116, 1089-1094, 10.1073/pnas.1811022116, 2019.

MacMartin, D. G., Kravitz, B., Tilmes, S., Richter, J. H., Mills, M. J., Lamarque, J.-F., Tribbia, J. J., and Vitt, F.: The Climate Response to Stratospheric Aerosol Geoengineering Can Be Tailored Using Multiple Injection Locations, Journal of Geophysical Research: Atmospheres, 122, 12,574-512,590, https://doi.org/10.1002/2017JD026868, 2017.

Mauritsen, T., Bader, J., Becker, T., Behrens, J., Bittner, M., Brokopf, R., Brovkin, V., Claussen, M., Crueger, T., Esch, M., Fast, I., Fiedler, S., Fläschner, D., Gayler, V., Giorgetta, M., Goll, D. S., Haak, H., Hagemann, S., Hedemann, C., Hohenegger, C., Ilyina, T., Jahns, T., Jimenéz-de-la-Cuesta, D., Jungclaus, J., Kleinen, T., Kloster, S., Kracher, D., Kinne, S., Kleberg, D., Lasslop, G., Kornblueh, L., Marotzke, J., Matei, D., Meraner, K., Mikolajewicz, U., Modali, K., Möbis, B., Müller, W. A., Nabel, J. E. M. S., Nam, C. C. W., Notz, D., Nyawira, S.-S., Paulsen, H., Peters, K., Pincus, R., Pohlmann, H., Pongratz, J., Popp, M., Raddatz, T. J., Rast, S., Redler, R., Reick, C. H., Rohrschneider, T., Schemann, V., Schmidt, H., Schnur, R., Schulzweida, U., Six, K. D., Stein, L., Stemmler, I., Stevens, B., von Storch, J.-S., Tian, F., Voigt, A., Vrese, P., Wieners, K.-H., Wilkenskjeld, S., Winkler, A., and Roeckner, E.: Developments in the MPI-M Earth System Model version 1.2 (MPI-ESM1.2) and Its Response to Increasing CO2, Journal of Advances in Modeling Earth Systems, 11, 998-1038, https://doi.org/10.1029/2018MS001400, 2019.

Monteith, J. L.: Evaporation and environment, Symposia of the Society for Experimental Biology, 19, 205-234, 1965.

Niemeier, U., Richter, J. H., and Tilmes, S.: Differing responses of the quasi-biennial oscillation to artificial SO2 injections in two global models, Atmos. Chem. Phys., 20, 8975-8987, 10.5194/acp-20-8975-2020, 2020.

Niemeier, U., Schmidt, H., Alterskjær, K., and Kristjánsson, J. E.: Solar irradiance reduction via climate engineering: Impact of different techniques on the energy balance and the hydrological cycle, Journal of Geophysical Research: Atmospheres, 118, 11,905-911,917, https://doi.org/10.1002/2013JD020445, 2013.

Odoulami, R. C., New, M., Wolski, P., Guillemet, G., Pinto, I., Lennard, C., Muri, H., and Tilmes, S.: Stratospheric Aerosol Geoengineering could lower future risk of 'Day Zero' level droughts in Cape Town, Environmental Research Letters, 15, 124007, 10.1088/1748-9326/abbf13, 2020.

Palmer, P. I., Wainwright, C. M., Dong, B., Maidment, R. I., Wheeler, K. G., Gedney, N., Hickman, J. E., Madani, N., Folwell, S. S., Abdo, G., Allan, R. P., Black, E. C. L., Feng, L., Gudoshava, M., Haines, K., Huntingford, C., Kilavi, M., Lunt, M. F., Shaaban, A., and Turner,

https://doi.org/10.5194/egusphere-2025-2266
Preprint. Discussion started: 28 May 2025

A. G.: Drivers and impacts of Eastern African rainfall variability, Nature Reviews Earth & Environment, 4, 254-270, 10.1038/s43017-023-00397-x, 2023.

Penman, H. L. and Keen, B. A.: Natural evaporation from open water, bare soil and grass, Proceedings of the Royal Society of London. Series A. Mathematical and Physical Sciences, 193, 120-145, 10.1098/rspa.1948.0037, 1948.

Pope, F. D., Braesicke, P., Grainger, R. G., Kalberer, M., Watson, I. M., Davidson, P. J., and Cox, R. A.: Stratospheric aerosol particles and solar-radiation management, Nature Climate Change, 2, 713-719, 10.1038/nclimate1528, 2012.

Ricke, K., Wan, J. S., Saenger, M., and Lutsko, N. J.: Hydrological Consequences of Solar Geoengineering, 51, 447-470, https://doi.org/10.1146/annurev-earth-031920-083456, 2023.

Ricke, K. L., Rowlands, D. J., Ingram, W. J., Keith, D. W., and Granger Morgan, M.: Effectiveness of stratospheric solar-radiation management as a function of climate sensitivity, Nature Climate Change, 2, 92-96, 10.1038/nclimate1328, 2012.

Rusca, M., Savelli, E., Di Baldassarre, G., Biza, A., and Messori, G.: Unprecedented droughts are expected to exacerbate urban inequalities in Southern Africa, Nature Climate Change, 13, 98-105, 10.1038/s41558-022-01546-8, 2023.

Samaniego, L., Thober, S., Kumar, R., Wanders, N., Rakovec, O., Pan, M., Zink, M., Sheffield, J., Wood, E. F., and Marx, A.: Anthropogenic warming exacerbates European soil moisture droughts, Nature Climate Change, 8, 421-426, 10.1038/s41558-018-0138-5, 2018.

Simpson, I. R., Tilmes, S., Richter, J. H., Kravitz, B., MacMartin, D. G., Mills, M. J., Fasullo, J. T., and Pendergrass, A. G.: The Regional Hydroclimate Response to Stratospheric Sulfate Geoengineering and the Role of Stratospheric Heating, Journal of Geophysical Research: Atmospheres, 124, 12587-12616, https://doi.org/10.1029/2019JD031093, 2019.

Smith, W.: The cost of stratospheric aerosol injection through 2100, Environmental Research Letters, 15, 114004, 10.1088/1748-9326/aba7e7, 2020.

Smith, W. and Wagner, G.: Stratospheric aerosol injection tactics and costs in the first 15 years of deployment, Environmental Research Letters, 13, 124001, 10.1088/1748-9326/aae98d, 2018.

Song, F. A.-O., Zhang, G. A.-O., Ramanathan, V., and Leung, L. A.-O.: Trends in surface equivalent potential temperature: A more comprehensive metric for global warming and weather extremes. LID - 10.1073/pnas.2117832119 [doi] LID - e2117832119,

Sun, F., Wang, T., and Wang, H.: Mapping Global GDP Exposure to Drought, in: Atlas of Global Change Risk of Population and Economic Systems, Springer Nature Singapore, Singapore, 123-130, 10.1007/978-981-16-6691-9_9, 2022.

Taylor, K. E.: Summarizing multiple aspects of model performance in a single diagram, Journal of Geophysical Research: Atmospheres, 106, 7183-7192, https://doi.org/10.1029/2000JD900719, 2001.

Tebaldi, C., Ranasinghe, R., Vousdoukas, M., Rasmussen, D. J., Vega-Westhoff, B., Kirezci, E., Kopp, R. E., Sriver, R., and Mentaschi, L.: Extreme sea levels at different global warming levels, Nature Climate Change, 11, 746-751, 10.1038/s41558-021-01127-1, 2021.

Thornthwaite, C. W.: An Approach toward a Rational Classification of Climate, Geographical Review, 38, 55-94, 10.2307/210739, 1948.

Tilmes, S., Mills, M. J., Niemeier, U., Schmidt, H., Robock, A., Kravitz, B., Lamarque, J. F., Pitari, G., and English, J. M.: A new Geoengineering Model Intercomparison Project

https://doi.org/10.5194/egusphere-2025-2266
Preprint. Discussion started: 28 May 2025

(GeoMIP) experiment designed for climate and chemistry models, Geosci. Model Dev., 8, 43-49, 10.5194/gmd-8-43-2015, 2015.

Tilmes, S., Richter, J. H., Kravitz, B., MacMartin, D. G., Mills, M. J., Simpson, I. R., Glanville, A. S., Fasullo, J. T., Phillips, A. S., Lamarque, J.-F., Tribbia, J., Edwards, J., Mickelson, S., and Ghosh, S.: CESM1(WACCM) Stratospheric Aerosol Geoengineering Large Ensemble Project, Bulletin of the American Meteorological Society, 99, 2361-2371, 10.1175/bams-d-17-0267.1, 2018.

Tilmes, S., Fasullo, J., Lamarque, J.-F., Marsh, D. R., Mills, M., Alterskjær, K., Muri, H., Kristjánsson, J. E., Boucher, O., Schulz, M., Cole, J. N. S., Curry, C. L., Jones, A., Haywood, J., Irvine, P. J., Ji, D., Moore, J. C., Karam, D. B., Kravitz, B., Rasch, P. J., Singh, B., Yoon, J.-H., Niemeier, U., Schmidt, H., Robock, A., Yang, S., and Watanabe, S.: The hydrological impact of geoengineering in the Geoengineering Model Intercomparison Project (GeoMIP), Journal of Geophysical Research: Atmospheres, 118, 11,036-011,058, https://doi.org/10.1002/jgrd.50868, 2013.

Tilmes, S., Visioni, D., Jones, A., Haywood, J., Séférian, R., Nabat, P., Boucher, O., Bednarz, E. M., and Niemeier, U.: Stratospheric ozone response to sulfate aerosol and solar dimming climate interventions based on the G6 Geoengineering Model Intercomparison Project (GeoMIP) simulations, Atmos. Chem. Phys., 22, 4557-4579, 10.5194/acp-22-4557-2022, 2022.

Trenberth, K. E., Dai, A., van der Schrier, G., Jones, P. D., Barichivich, J., Briffa, K. R., and Sheffield, J.: Global warming and changes in drought, Nature Climate Change, 4, 17-22, 10.1038/nclimate2067, 2014.

UNDP: Human Development Report 2023/2024 : breaking the gridlock - reimagining cooperation in a polarized world, New York, 2024.

van der Schrier, G., Barichivich, J., Briffa, K. R., and Jones, P. D.: A scPDSI-based global data set of dry and wet spells for 1901–2009, Journal of Geophysical Research: Atmospheres, 118, 4025-4048, https://doi.org/10.1002/jgrd.50355, 2013.

Visioni, D., MacMartin, D. G., Kravitz, B., Boucher, O., Jones, A., Lurton, T., Martine, M., Mills, M. J., Nabat, P., Niemeier, U., Séférian, R., and Tilmes, S.: Identifying the sources of uncertainty in climate model simulations of solar radiation modification with the G6sulfur and G6solar Geoengineering Model Intercomparison Project (GeoMIP) simulations, Atmos. Chem. Phys., 21, 10039-10063, 10.5194/acp-21-10039-2021, 2021.

Wang, T. and Sun, F.: Global gridded GDP data set consistent with the shared socioeconomic pathways, Scientific Data, 9, 221, 10.1038/s41597-022-01300-x, 2022.

Wells, N., Goddard, S., and Hayes, M. J.: A Self-Calibrating Palmer Drought Severity Index, Journal of Climate, 17, 2335-2351, https://doi.org/10.1175/1520-0442(2004)017<2335:ASPDSI>2.0.CO;2, 2004.

Wilson, J. C., Jonsson, H. H., Brock, C. A., Toohey, D. W., Avallone, L. M., Baumgardner, D., Dye, J. E., Poole, L. R., Woods, D. C., DeCoursey, R. J., Osborn, M., Pitts, M. C., Kelly, K. K., Chan, K. R., Ferry, G. V., Loewenstein, M., Podolske, J. R., and Weaver, A.: In Situ Observations of Aerosol and Chlorine Monoxide After the 1991 Eruption of Mount Pinatubo: Effect of Reactions on Sulfate Aerosol, Science, 261, 1140-1143, 10.1126/science.261.5125.1140, 1993.

Yue, X., Tian, C., and Lei, Y.: Relieved drought in China under a low emission pathway to 1.5°C global warming, International Journal of Climatology, 41, E259-E270, https://doi.org/10.1002/joc.6682, 2021.

https://doi.org/10.5194/egusphere-2025-2266
Preprint. Discussion started: 28 May 2025

Zhang, W., Zhou, T., and Wu, P.: Anthropogenic amplification of precipitation variability over the past century, Science, 385, 427-432, 10.1126/science.adp0212, 2024.
Zhou, L., Tian, Y., Myneni, R. B., Ciais, P., Saatchi, S., Liu, Y. Y., Piao, S., Chen, H., Vermote, E. F., Song, C., and Hwang, T.: Widespread decline of Congo rainforest greenness in the past decade, Nature, 509, 86-90, 10.1038/nature13265, 2014.

https://doi.org/10.5194/egusphere-2025-2266
Preprint. Discussion started: 28 May 2025

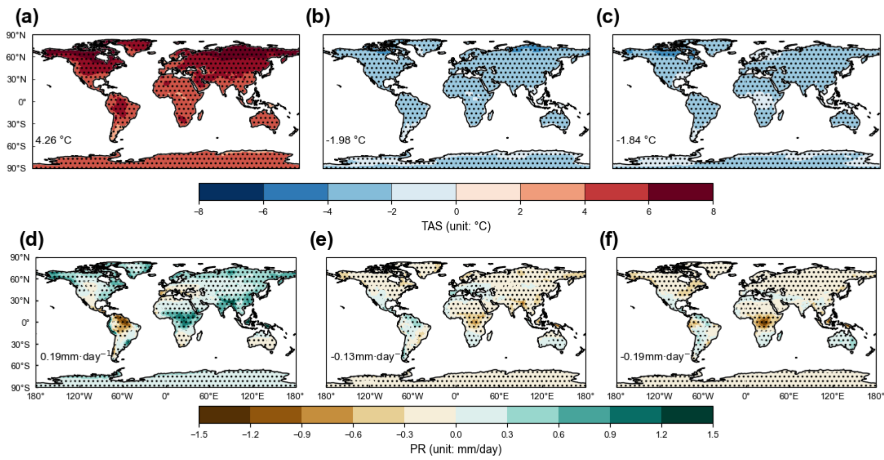

Figure 1. Climatic responses to global warming and SRM in GeoMIP. Results shown are the spatial pattern of annual mean changes in (a, b, c) temperature and (d, e, f) precipitation at 2081-2100 under (a, d) SSP5-8.5 scenario relative to the historical period of 1995-2014, as well as that under (b, e) G6solar and (c, f) G6sulfur scenarios relative to SSP5-8.5 both at 2081-2100. The dotted areas indicate regions where at least four out of five models show changes with the same signs. The global mean value of the difference is shown at the lower-left of each panel. Climatic responses to GLENS are presented in Figure S2.

https://doi.org/10.5194/egusphere-2025-2266
Preprint. Discussion started: 28 May 2025

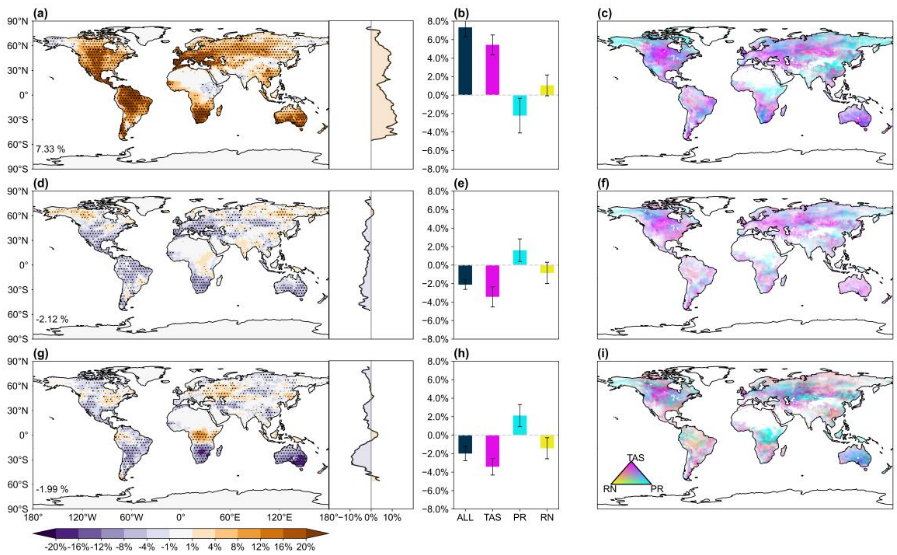

Figure 2. Changes in frequency of drought extremes by global warming and SRM in GeoMIP. Results shown are the changes in frequency of drought extremes (scPDSI < -4) at 2081-2100 under (a) SSP5-8.5 scenario relative to the historical period of 1995-2014, as well as that under (d) G6solar and (g) G6sulfur scenarios relative to SSP5-8.5 both at 2081-2100. The dotted areas indicate regions where at least four out of five models show changes with the same signs. Latitudinal distribution is shown on the right of each panel. Contributions of temperature (TAS), precipitation (PR), and radiation (RN) to changes in drought extremes are also presented, with bars in (b, e, h) representing the mean and errorbars indicating one standard deviation of predictions from five GeoMIP models. Colors in (c, f, i) indicate the dominant drivers of drought extremes.

https://doi.org/10.5194/egusphere-2025-2266
Preprint. Discussion started: 28 May 2025

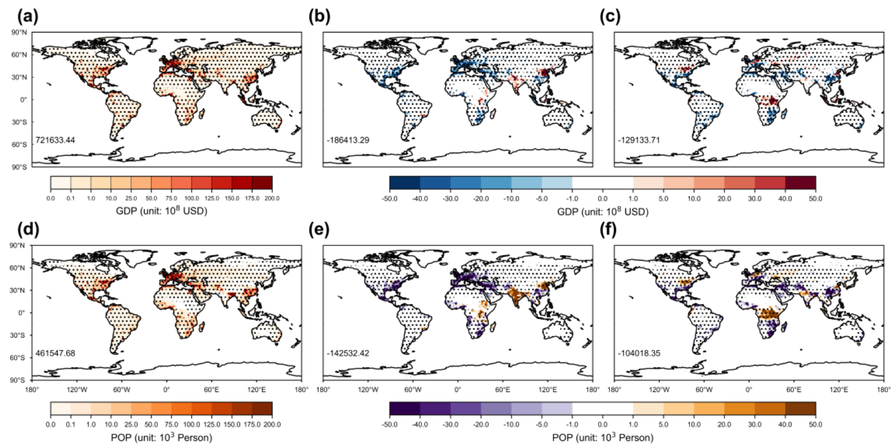

Figure. 3. Changes in GDP and population exposure to drought extremes. Results shown are the changes of (a, b, c) GDP and (c, d, f) population (POP) exposure to drought extremes at 2081-2100 (a, d) under SSP5-8.5 scenario relative to the historical period of 1995-2014, as well as that (b, e) under G6solar and (c, f) G6sulfur scenarios relative to SSP5-8.5 both at 2081-2100. The dotted areas indicate regions where at least four out of five models show changes with the same signs. The global sum value of the difference is shown at the lower-left of each panel.

https://doi.org/10.5194/egusphere-2025-2266
Preprint. Discussion started: 28 May 2025

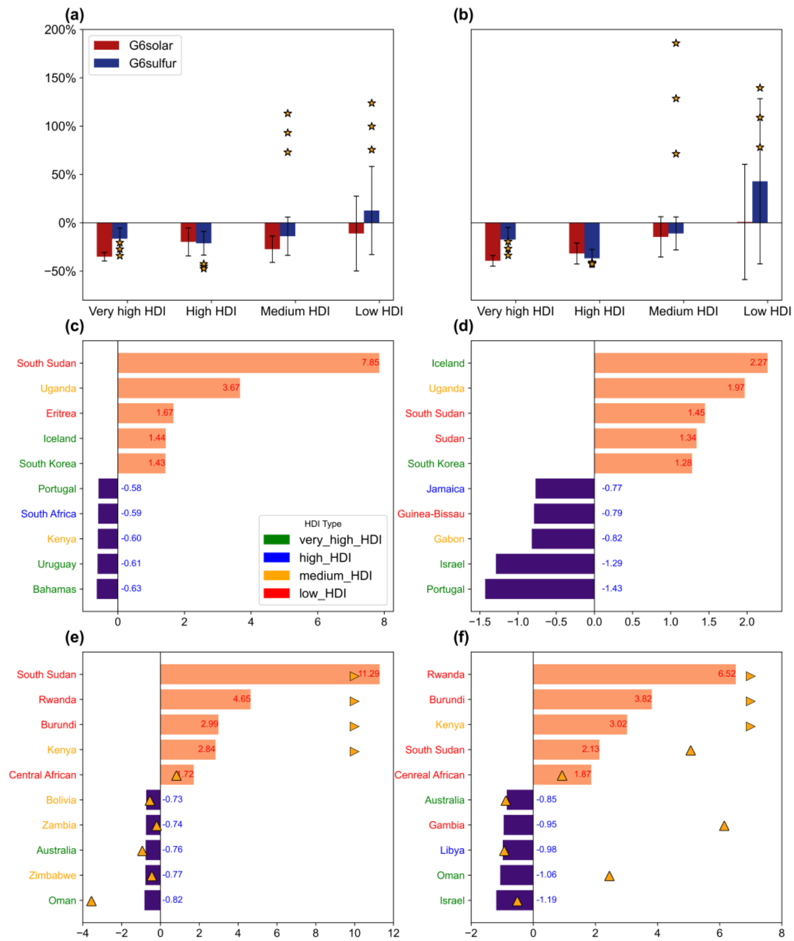

Figure. 4. Changes in GDP and population exposure to drought extremes by HDI. For each of four HDI groups, changes in (a) GDP or (b) population exposure to drought extremes for 2081-2100 in G6solar (blue) and G6sulfur (red) relative to SSP5-8.5 are normalized by the differences under SSP5-8.5 relative to 1995-2014. The bars represent the mean changes from five models with errorbars indicating one standard deviation for inter-model spread. Yellow stars represent results from three members of GLENS. The mitigation potential (MP, see Methods) is also calculated for individual countries, and the top 5 countries with the greatest mitigation (violet) or aggravation (orange) of (c, e) GDP and (d, f) population exposures to drought extremes are shown for (c, d) G6solar and (e, f) G6sulfur, respectively. The MP values (ratios of changes) are denoted for those top countries. Yellow triangles denote GLENS outcomes (right-aligned for values exceeding axis limits).